Computational Mechanics 20 (1997) 34–40 © Springer-Verlag 1997

The Gurson-Tvergaard-Needleman-model for rate and temperature-dependent materials with isotropic and kinematic hardening

S. Hao, W. Brocks

Abstract Based on the upper bound solution of cell models under dynamic or creep loading conditions, the Gurson-Tvergaard-Needleman (GTN) constitutive law of ductile fracture for rate and temperature-dependent materials with isotropic and kinematic hardening has been established. Two additional parameters, which account for the influences of strain rate, inertia and the average distance between voids, have been introduced in the GTN yield criterion. 2D and 3D analysis has been performed for different metals. It can be concluded that the GTN model is a powerful tool for crack growth analysis.

1
Introduction

Cell models are usually applied in two ways. The cell can represent the smallest material unit that contains sufficient information of the failure process in a material. In this case the dimensions of the cell must match the corresponding microscope features of the material. Alternatively, the cell can be considered as a structure in microscale within the material. Solutions obtained for the cell can be used to rationally link microscopic properties and mesoscopic quantities, so as to establish a general macroscale constitutive law for a damaged material in the frame of continuum medium mechanics. The present work considers the latter technique.

It has been observed experimentally that the dominant processes of ductile fracture are void nucleation, growth and coalescence. Based on the analysis of the upper-bound solutions for the cells within a cylindrical and a spherical void in a perfectly plastic material, Gurson has established constitutive equations (i.e. a yield condition and a flow rule) for porous materials which depend on the void volume fraction as a additional internal variable. This model has been further developed and modified by Tvergaard with respect to the yield condition and damage evolution (Tvergaard 1981, 1982; Tvergaard and Needleman 1984), and by Needleman to include the law of void nucleation (Needleman 1987; Chu and Needleman 1980). It will, therefore, be referenced as the Gurson-Tvergaard-Needlemen (GTN) model in the following. The yield function and plastic potential in the GTN model are expressed as:

$$\Phi = \left(\frac{\Sigma}{\sigma_0}\right)^2 + 2q_1 f^* \cdot ch\left(\frac{3q_2\Sigma_m}{2\sigma_0}\right) - 1 - q_3 f^{*^2} \qquad (1)$$

where Σ and Σ_m denote he Mises stress and hydrostatic stress on the mesoscopic scale; $q_1 = 1.5, q_2 = 1, q_3 = 2.25$ (Tvergaard 1981, 1982) and σ_0 represents the yield strength of the matrix. In (1) the modified damage parameter f^* is related to the void volume fraction f by taking account of the accelerated process of coalescence after reaching a critical void volume fraction, f_c (Tvergaard 1981; Needleman 1987).

Due to the high nonlinearity of the problem the analysis of damage is usually restricted to quasi-static and monotonic loading and isothermal conditions, considering the material to be and to remain isotropic. The rate and temperature dependence of the mechanical behaviour and the production of heat due to plastic deformation are neglected. However, the effects of loading rate and temperature change as well as kinematic hardening due to cyclic deformation can be important in practice.

A numerical algorithm based on the Euler backward method has been developed for a class of pressure-dependent plasticity models by Aravas in 1987. For rate dependent solids, a one step forward gradient time integration scheme was developed by Peirce et al. (1984). Without the Tvergaard and Needleman modifications accounting for the effect of void coalescence and stress controlled nucleation, Pan et al. (1983) proposed a simple empirical equation for the strain rate and temperature dependence of the matrix material. This relationship was used by Needleman and Tvergaard (1991) for the numerical simulation of ductile fracture in isotropic materials under dynamic loading. Brocks et al. (1995) studied the transferability of the damage parameters for visco-plastic materials by numerical cell-model calculations.

In the present report, a generalization of the GTN model for a rate, temperature and pressure-dependent material with mixed hardening (i.e. combined isotropic and kinematic hardening) is described based on the analysis of cell models. The algorithm has been written as a user subroutine (UMAT) for the ABAQUS code (1994). To check the accuracy and efficiency of the code, single element numerical tests have been carried out and thereafter 2D and 3D examples have been treated. In the following analysis the standard notion adopted in Gurson (1977) and Peirce et al. (1984) is used.

Communicated by P. E. O'Donoghue, M. D. Gilchrist, K. B. Broberg, 6 January 1997

S. Hao, W. Brocks
Institute of Material Research, GKSS Research Center,
TD-21502 Geesthacht, Germany

The grant from Deutsche Ferschungsgemeinschaft (DFG) is appreciated.

2
Constitutive relations

2.1
Dynamic loading

Usually the strain rate of the matrix material can be decomposed as:

$$\dot{\varepsilon}_{ij}^{total} = \dot{\varepsilon}_{ij}^{e} + \dot{\varepsilon}_{ij}^{vp} + \dot{\varepsilon}_{ij}^{t} \qquad (2)$$

where the superscripts "e" and "vp" denote the elastic and viscoplastic components and the superscript "t" represents the contribution to strain rate due to thermal expansion.

The associated flow rule, i.e. the relation between microscopic stress and viscoplastic strain under dynamic loading, is written as (Perzyna 1966; Gilat and Clifton 1985):

$$\dot{\varepsilon}_{ij}^{vp} = \dot{\varepsilon}^{vp}\frac{\partial F}{\partial \sigma_{ij}} \qquad (3)$$

with

$$\left.\begin{array}{l} F = \sigma = \left[\frac{3}{2}\sigma'_{ij}\sigma'_{ij}\right]^{1/2} \\ \quad \text{(Von Mises yield function)} \\ \dot{\varepsilon}^{vp} = \left[\frac{2}{3}\dot{\varepsilon}_{ij}^{vp}\dot{\varepsilon}_{ij}^{vp}\right]^{1/2} \;; \\ \varepsilon^{vp} = \int_0^t \dot{\varepsilon}^{vp}\mathrm{d}t \text{ and } \sigma'_{ij} = \sigma_{ij} - \frac{1}{3}\delta_{ij}\sigma_{kk} \end{array}\right\} \qquad (4)$$

The visco-plastic strain rate relation can be expressed as follows (Pan et al. 1983; Needleman and Tvergaard 1991):

$$\frac{\sigma}{g(T, \varepsilon^{vp})} = \left[\frac{\dot{\varepsilon}^{vp}}{\dot{\varepsilon}_0^{vp}}\right]^{\kappa} \qquad (5)$$

where $\dot{\varepsilon}_0^{vp}$ is a reference strain rate, κ is a material constant and $g(T, \varepsilon^{vp})$ specifies the strain hardening characteristics and their dependence on temperature T.

Under adiabatic conditions, from the energy balance $\dot{\boldsymbol{\varepsilon}}^t$ (the part of strain rate tensor due to temperature change) is determined by (Needleman and Tvergaard 1991)

$$\dot{\varepsilon}^t = \alpha\dot{T}\mathbf{I} \quad \text{and} \quad \rho c\dot{T} = 0.9\,\boldsymbol{\sigma} : \dot{\boldsymbol{\varepsilon}}^{vp} \qquad (6)$$

where α is the thermal expansion coefficient, $\mathbf{I}$ denotes a unit tensor, c and ρ represent the heat capacity and density of the reference configuration.

In a kinematic strain hardening material, the back stress tensor $\boldsymbol{\alpha}$ is introduced as an additional internal tensor variable which relates the shifted stress tensor $\mathbf{b}$, to the total stress $\boldsymbol{\sigma}$, by $\mathbf{b} = \boldsymbol{\sigma} - \boldsymbol{\alpha}$. Thus, the flow potential F and the effective stress σ in (4) are defined by:

$$F = \sigma = \left[\frac{3}{2}(\sigma'_{ij} - \alpha_{ij})(\sigma'_{ij} - \alpha_{ij})\right]^{1/2} \qquad (7)$$

Ziegler's hardening rule is employed in the analysis:

$$\dot{\alpha}_{ij} = \mu\dot{\varepsilon}^{vp}\frac{\partial F}{\partial \sigma_{ij}} = \mu\dot{\varepsilon}^{vp}\frac{3(\sigma'_{kl} - \alpha_{kl})}{2\sigma} \qquad (8)$$

where μ is a scalar function determined from the uniaxial static stress-strain curve (Gilat and Clifton 1985).

2.2
Creep

Experimental observations (Riedel 1986) reveal that damage by means of void growth and coalescence at grain boundaries can dominate the process of creep failure. In this case the total strain rate is decomposed as the sum of four different parts:

$$\dot{\varepsilon}_{ij}^{total} = \dot{\varepsilon}_{ij}^{e} + \dot{\varepsilon}_{ij}^{p} + \dot{\varepsilon}_{ij}^{c} + \dot{\varepsilon}_{ij}^{t} \qquad (9)$$

The plastic strain rate, $\dot{\varepsilon}_{ij}^{p}$, can be determined by the rate independent Prandtl-Reuss flow rule. The first relation in (6) can be used to determine the thermal strain rate contribution in general. The creep strain rate can be expressed generally as in Riedel (1986)

$$\dot{\varepsilon}_{ij}^{c} = \dot{\varepsilon}^{c}\left\{F_{C1}b'_{ij} + F_{C2}\sigma_I m_{ij}\right\} \qquad (10)$$

where σ_I represents the maximum principal stress. F_{C1} and F_{C2} are functions of i) σ_I, ii) equivalent stress σ, iii) damage and iv) material constants. The tensor m_{ij} is defined such that its components in the co-ordinate system of the principal axes of stress are zero except in the direction of σ_I where $m_{II} = 1$.

A simple form of (10) has been suggested by Kachanov (1961) with

$$F_{C1} = \left[\frac{\sigma}{(1-\omega)\sigma_0}\right]^{N_c}\frac{3}{2\sigma}; \quad F_{C2} = 0 \qquad (11)$$

where ω denotes the creep damage, σ denotes the effective stress, N_c and σ_0 are material constants.

3
Micromechanics and cell modelling

3.1
Average of microscopic quantities

As mentioned above, the temperature and strain rate-dependence as well as the anisotropy have non-negligible effects on the evolution of damage. To consider these effects a "cell model", which represents a very small unit of a solid body, has been used to establish the relationship between microscopic and mesoscopic behaviour, see Fig. 1. A representative volume element (V) of a material containing a volume of cavities, V^*, is subjected to mesoscopic stresses $\boldsymbol{\Sigma}$ or strain rate $\dot{\boldsymbol{\Sigma}}$ which induce microscopic stresses $\boldsymbol{\sigma}$ (or $\mathbf{b}$) and strain rate $\dot{\varepsilon}$ at every point in V. From the balance of energy mesoscopic quantities can be expressed as the volume averages of the microscopic quantities (Gurson 1977):

$$\dot{E}_{ij} = \frac{1}{V}\int_v \dot{\varepsilon}_{ij}\,\mathrm{d}V \qquad (12)$$

$$\Sigma_{ij} = \frac{1}{V}\int_v \sigma_{kl}\frac{\partial\dot{\varepsilon}_{kl}}{\partial\dot{E}_{ij}}\,\mathrm{d}V \qquad (13)$$

In the following analysis we usually adopt, unless otherwise indicated, small letters to symbolize the quantities in micro-scale and capitals for the quantities in macro-scale. Using (13) one may also define the mesoscopic total, shifted and back stresses, $\boldsymbol{\Sigma}, \mathbf{B}$, and $\mathbf{A}$. Thus one obtains:

$$\Sigma = \left[\frac{3}{2}B'_{ij} : B'_{ij}\right]^{\frac{1}{2}}; \quad \Sigma_m = \frac{\mathrm{tr}(\boldsymbol{\Sigma})}{3} \text{ and } B_{ij} = B'_{ij} - \delta_{ij}\Sigma_m \tag{14}$$

For rigid perfectly-plastic material, the upper-bound solutions of the cells in Fig. 1 have been given in Gurson (1977). Under dynamic condition, the solution of a spherical cell as shown in Fig. 1a has been discussed in Johnson (1981) and Freund (1992).

3.2
Cell model analysis: the dynamic solution of the cylindrical cell model in Fig. 1b

In the analysis we shall neglect the effects of global acceleration and velocity. In general the constitutive law and the momentum balance equations can be expressed as a set of first order partial differential equations:

$$\left.\begin{aligned} &\overset{\nabla}{\boldsymbol{\sigma}} = \boldsymbol{L} : \dot{\boldsymbol{\varepsilon}}^{total} \\ &\nabla\boldsymbol{\sigma} = \rho\frac{Dv}{Dt} \end{aligned}\right\} \tag{15}$$

where $\overset{\nabla}{\boldsymbol{\sigma}}$ and $\boldsymbol{L}$ are the Jaumann stress rate tensor and the tangent matrix of the material, respectively. t represents time and Dv/Dt denotes the material derivative of the velocity field v. Generally speaking, for partial equations like (15) a characteristic analysis can be applied. Considering the simple case of general plane symmetric deformation and leaving out the effect of temperature change caused by plastic dissipation, one has:

$$\begin{aligned} &\dot{\varepsilon}_{rr} = \frac{\mathrm{d}v_r}{\mathrm{d}r}, \quad \dot{\varepsilon}_{\theta\theta} = \frac{v_r}{r}, \quad \dot{\varepsilon}_{zz} = \text{const}, \\ &\quad v_\theta = \dot{\varepsilon}_{r\theta} = \dot{\varepsilon}_{rz} = \dot{\varepsilon}_{\theta z} = 0 \end{aligned} \tag{16}$$

The boundary conditions of the cell in Fig. 1b are given as follows:

$$\left.\begin{aligned} &v_r(r) = 0, \quad \text{for all } r \in \{a_0, b_0\}; \\ &\quad a = a_0; \quad b = b_0; \quad \text{when } t < 0 \\ &v_r(b) = k\dot{E}_0 : \ a = a(t); \ k : const. \\ &\quad b = b(t); \qquad\qquad \text{when } t \geq 0 \end{aligned}\right\} \tag{17}$$

Using the differential operation in the reference configuration that coincides with the current configuration at time t, the Eq. (15) can be expressed as:

$$\left.\begin{aligned} &\frac{\partial\sigma_{rr}}{\partial t} = K_{rr}\frac{\partial v_r}{\partial r} + K_{\theta\theta}\frac{v_r}{r} + K_{zz}\dot{\varepsilon}_{zz} \quad \text{with } K_{ij} = L_{rrij} \\ &\frac{\partial\sigma_{rr}}{\partial r} + \frac{\sigma_{rr} - \sigma_{\theta\theta}}{r} = \rho\frac{\partial v_r}{\partial t} \end{aligned}\right\} \tag{18}$$

The system (18) possesses two families of characteristics in the $\{r, t\}$ plane

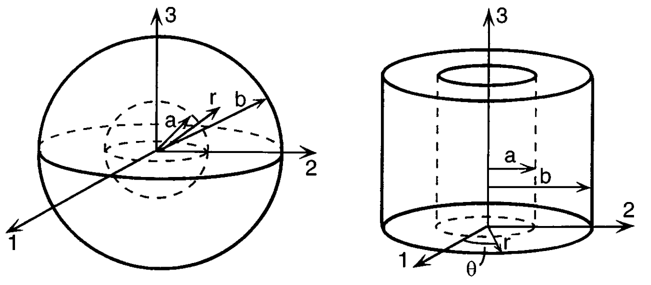

a Spherical void model b Long circular cylindrical cell model

Fig. 1a,b. The analysed cell models. **a** spherical void model; **b** long circular cylindrical cell model

$$\frac{\mathrm{d}t}{\mathrm{d}r} = \pm\sqrt{\rho K_{rr}} \tag{19}$$

A negative sign in (19) represents the wave front moving toward the cylinder center. The positive sign represents the reverse wave movement, as illustrated in Fig. 2. The solutions of (18) can be obtained by integration along the characteristics as described by (19). For application, the time scale t^* in Fig. 2 may be important because it denotes the instance that the cell is in a fully plastic state. Thus, the value of $(2b_0)/t^*$ represents the expansion speed of the plastic zone in the porous material. In the reference configuration which coincides to the current configuration at $t = t^*$, from incompressibility of the material an upper-bound velocity field is:

$$\begin{aligned} &v_r = \frac{b^2\dot{E}_0}{2r} - \frac{r\dot{E}_{33}}{2}; \quad v_\theta = 0 \\ &\quad \text{with } \dot{E}_0 = \frac{2\dot{E}_{11} + \dot{E}_{33}}{2}; \quad \dot{E}_{11} = \dot{E}_{22} = \frac{\dot{E}_{33}}{k_3} \end{aligned} \tag{20}$$

where k_3 is a constant. Substituting (20) into the second relation of (18) one obtains:

$$\begin{aligned} &\sigma_{rr}(r) = R_I + R_{II} \\ &\quad \text{with } R_I = \int_a^r \frac{2\sigma}{3\dot{\varepsilon}}\left[\frac{\dot{\varepsilon}_{\theta\theta} - \dot{\varepsilon}_{rr}}{r}\right]\mathrm{d}r; \ R_{II} = \rho\int_a^r \frac{\partial v_r}{\partial t}\,\mathrm{d}r \end{aligned} \tag{21}$$

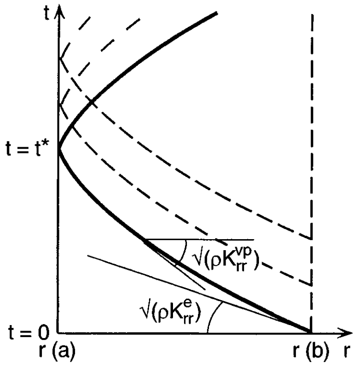

Fig. 2. Illustration of the "wave front" in the cell using characteristic analysis

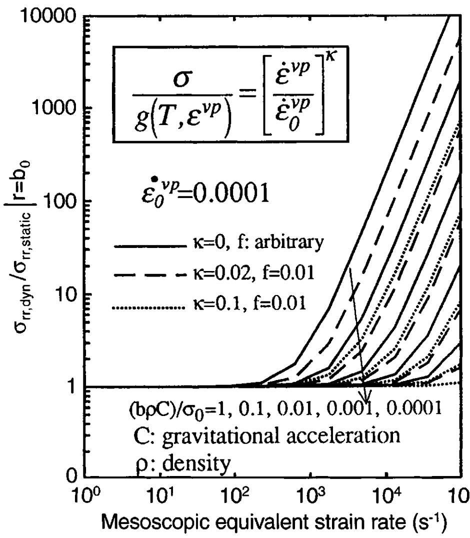

Fig. 3. Stress increase due to inertia at the outside surface of the cell

where R_I is due to the viscoplastic part and R_{II} refers to the effect of inertia. Using (5) and (20) it is not difficult to derive the explicit expressions of R_I and R_{II}. Fig. 3 illustrates relationships between the mesoscopic equivalent strain rate $\dot{E}$ and the function $\eta_H(b_0)$ which is defined by:

$$\eta_H(b_0) = \frac{\sigma_{rr}|_{r=b_0,\, dynamic}}{\sigma_{rr}|_{r=b_0,\, static}} \qquad (22)$$

From (20) the mesoscopic stresses can be expressed as below, using (12) and (13):

$$\Sigma = \frac{\sqrt{3}}{2V}\int_v \sigma \dot{E}_{33}\Psi\,\mathrm{d}V;\quad \Sigma_m = \frac{2}{V\sqrt{3}}\int_v \frac{\sigma\eta_H\dot{E}b^4}{r^4}\Psi\,\mathrm{d}V$$

$$\text{with } \Psi = \left[\frac{\dot{E}^2 b^4}{r^4} + \frac{3}{4}\dot{E}_{33}^2\right]^{-\frac{1}{2}} \qquad (23)$$

where σ is given by (5) with:

$$g(T,\varepsilon^{vp}) = \sigma_0[1-\beta(T-T_0)]\left[\frac{\varepsilon^{vp}}{\varepsilon_0^{vp}}\right]^N \qquad (24)$$

where β, N and σ_0 are material constants; the subscript “0” refers to the quantities at a given reference condition (Needleman and Tvergaard 1991).

The integrals in (23) have been solved numerically by using the mid-value theorem of integration. Thus the mesoscopic yield function has the form:

$$\Phi = \left(\frac{\Sigma}{\Sigma_{YI}}\right)^2 + 2q_1 f^* ch\left(-\frac{3q_2\Sigma_m}{2\Sigma_{Y2}}\right) - 1 - q_3 f^{*^2} \qquad (25)$$

with

$$\Sigma_{Yi} = \eta_i g(T,\dot{E})\ ;$$

$$\eta_i = \eta_i(f,\dot{E},b_0,T,\varepsilon^{vp},\text{material constants});\quad i = 1,2\ ;$$

The η_i are displayed in Fig. 4a as functions of f under quasi-static loading condition. The numerical results for the material model described by (5) and (24) show that:

$$\eta_1 \approx \eta_1|_{\text{quasi-static}};\quad \eta_2 \approx \eta_2|_{\text{quasi-static}}\eta_H(b_0) \qquad (26)$$

where b_0 is the outside radius of the cell. The value of $2b_0$ accounts for the “average distance between voids” in an actual material. Σ_{Yi} refer to, phenomenally, the “mesoscopic shear yield strength and volume expansion strength of the porous material”. Fig. 4b illustrates the change of the yield surface due to visco-plasticity.

In creep, if the cylindrical cell in the matrix can be described by (10) with $F_{C2} = 0$, a similar expression to (25) can be obtained (Hao and Brocks 1996).

4
Numerical examples and verification by experimental tests

Algorithms for the material characterized by the GTN model (25) have been developed and the corresponding numerical procedure has been implemented into the

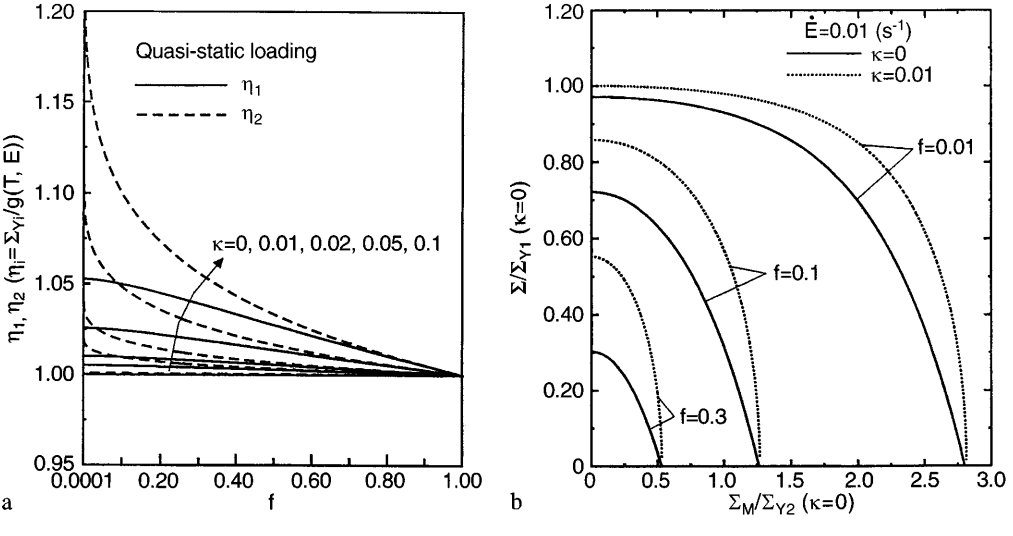

Fig. 4. **a** Dependence of η_1 and η_2 on f, calculated using the cell model; **b** Influence of rate-dependence on yield surface

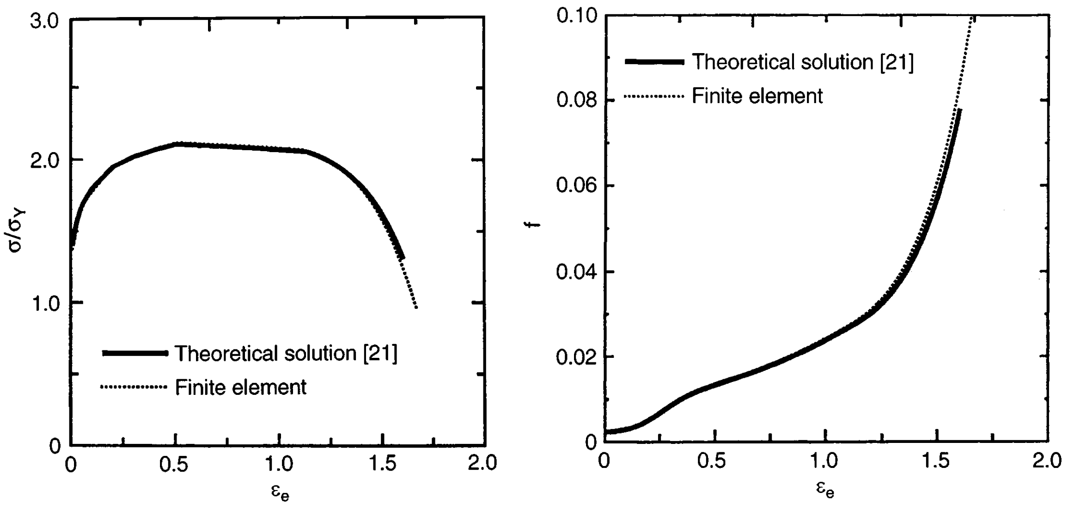

Fig. 5. Results of single element test: axial symmetric tension

"ABAQUS code (1994) as a "user subroutine". Single element tests of axial symmetric tensile and triaxial loading have been performed and compared to the analytical solutions that are given in Aravas (1987) and Aravas and McMeeking (1985) for rate-independent material. One example is displayed in Fig. 5. Simulation of the dynamic tensile bar, the cracked four point bend specimen (Brocks et al. 1996), the 3D Double Edge Cracked Tensile Panel (DET) and the Middle Cracked Tensile Panel (MT) have also been performed.

4.1
Round bar under static and dynamic tension

Studies of the necking behaviour of axi-symmetric specimens made of a 22NiMoCr37 ferritic steel under static and dynamic loading have been performed as verification tests. The numerical results gave a good prediction of the load vs. displacement curve and load vs. necking curve when compared with the static test result and the results are listed in Hao and Brocks (1996). The dynamic tests were carried out in the Frauhofer Institute of Materials Research at room temperature and −60 degrees (C) (Bernauer 1995). In order to verify the numerical procedure developed in the present work, the simulation has also been carried out for a dynamic tensile bar at room temperature. Under dynamic loading the movement of the stress wave is no longer symmetrical about the middle section, thus the element mesh shown in Fig. 6a has been used in the simulation. The whole test process took only 0.00585 seconds so that an adiabatic process can be assumed in the numerical simulation. Fig. 6b and 6c illustrate the contours of damage and temperature during necking. Fig. 7 displays a comparison between the numerical results and the test results for the load-time curve. It has been found in the analysis that the compliance of the dynamic test equipment has a significant effect on the amplitude of the stress wave.

4.2
Four point bending specimen, GGG nodular cast iron (Brocks et al. 1996)

Simulations of the behaviour of single edge notch four point bending specimens have been performed using the described user supplied routine. Tests on specimens made of two GGG-40 materials with different graphite morphologies have been performed at the IEHK Aachen and

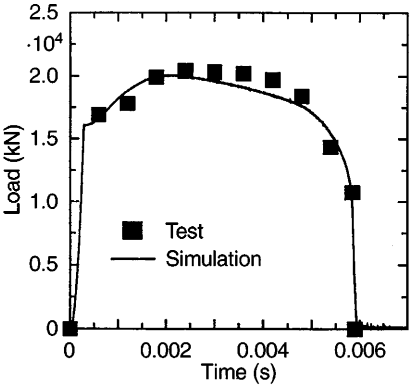

Fig. 7. Simulation of the impact tension bar

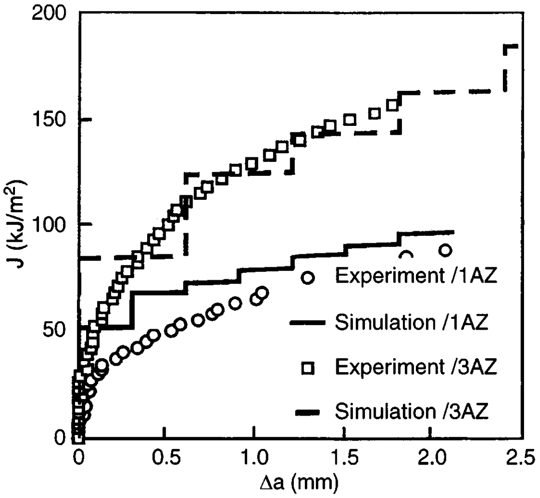

Fig. 8. J_R curves of GGG-1AZ1 & -3AZ

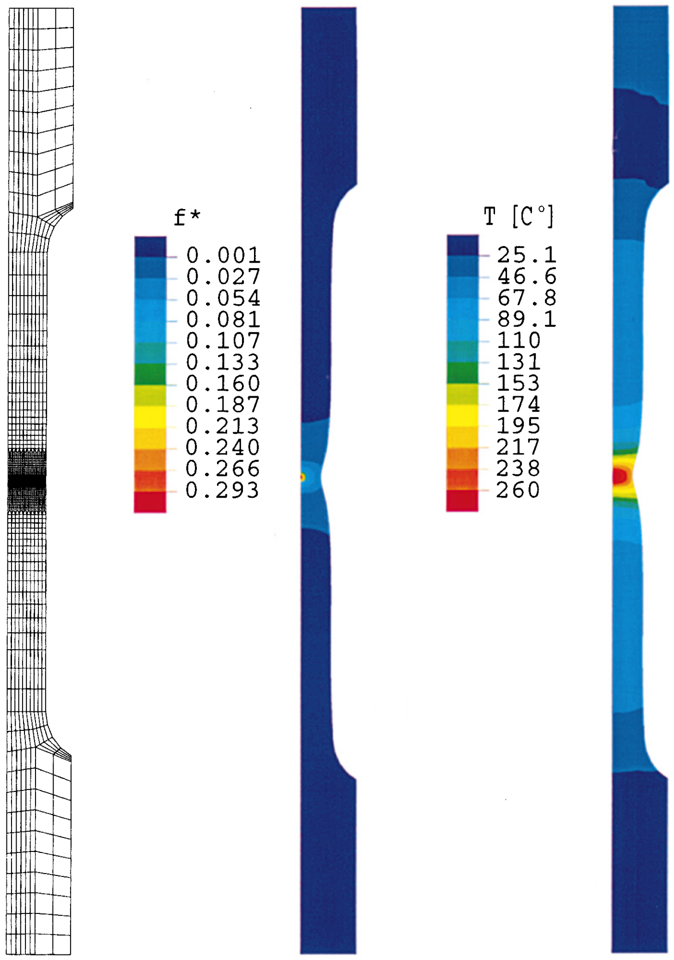

a Mesh b Damage c Temperature

Fig. 6. Illustration of the FE-simulation of the impact tension bar

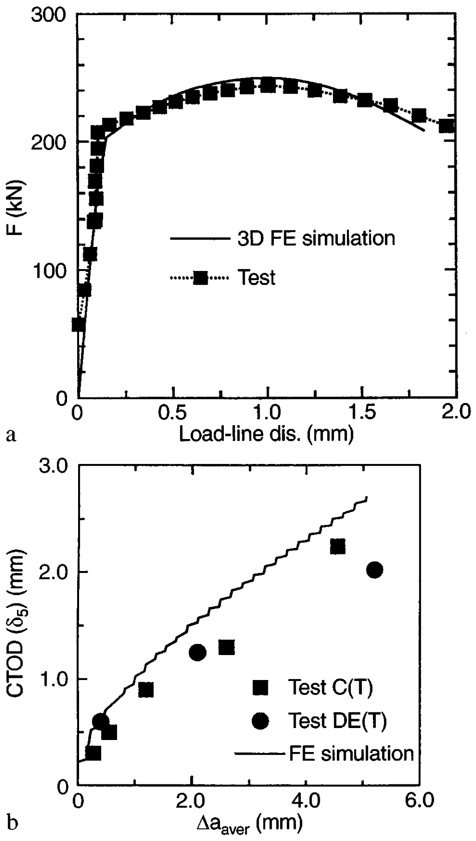

Fig. 9. Simulation of 3D DE(T) specimen

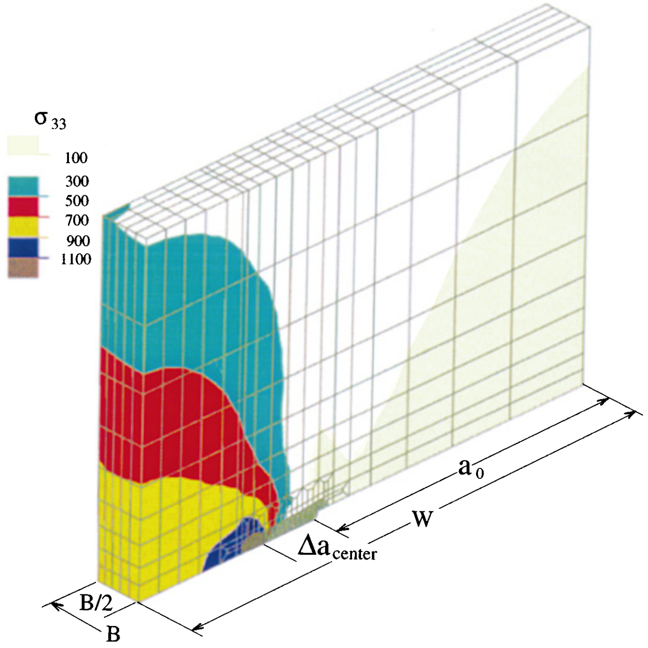

Fig. 10. Distribution of tensile stress, σ_{33}, in the DE(T) at $\Delta a_{\text{aver}} \approx 4.3\,\text{mm}$

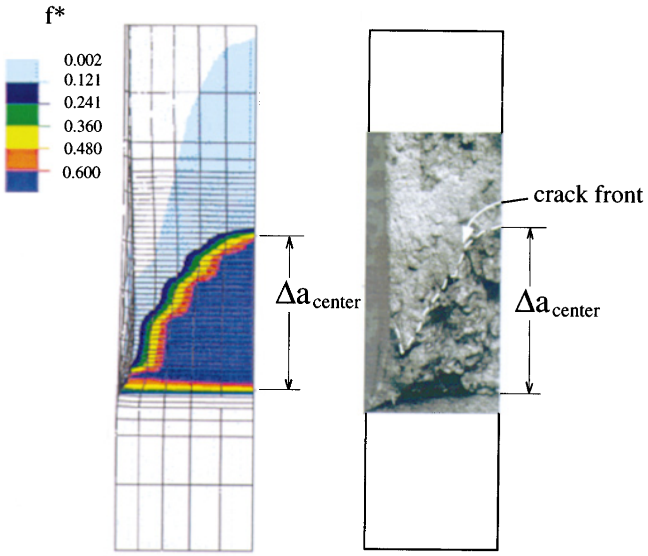

Fig. 11. Damage in the ligament (FE simulation) and ductile crack growth (experiment)

the TU Mining Academy Freiberg to provide the experimental data. A detailed description of the investigation is found in Brocks et al. (1996). Figure 8 shows a comparison of the experimental and numerical J_R curves.

4.3
DE(T) specimen, 3D simulation

The ferritic pressure vessel steel 20 Mn Mo Ni 5 5 has been studied. Its strength and toughness properties have been characterized by tensile tests on round bars and fracture mechanic tests on C(T), DE(T) and M(T) specimens (Heerens et al. 1991). As the fracture mechanic specimens were not side grooved, three dimensional calculations appeared to be necessary. Due to a threefold symmetry only one eighth of the DE(T) had to be modelled. Figure 9a shows that the experimental and numerical load (F) vs elongation (ΔL) curves for the DE(T) specimen agree well. The crack growth resistance which is characterized by CTOD (δ_5) vs Δa curves are shown in Fig. 9b. Figure 10 displays normal stress contours in the tensile direction, σ_{33}, at the centre plane of the DE(T) specimen, and shows that the stress concentration takes place at the actual crack tip. The model can also realistically simulate the thumb nail shape of the crack growth. This is shown in Fig. 11 which compares the damage in the ligament obtained by the FE simulation (left) with the experimental crack growth front (right).

5
Summary

The upper bound solutions for a cylindrical unit cell with rate and temperature-dependent matrix materials have been investigated. The mesoscopic response of the cells has been used to establish the mesoscopic yield criterion, which has been expressed in the form introduced by Gurson, Tvergaard and Needleman. Two additional parameters appear in the GTN yield criterion, which represent the influences of strain rate, temperature, the average distance between voids and material inertia. Numerical examples and verifications of the model have been given.

References

Gurson, A. L. (1977) Continuum Theory of Ductile Rupture by Void Nucleation and Growth: Path I-Yield Function and Flow Rules for Porous Ductile Media. ASME Transaction, J. Eng. Mat. Tech. 99, 2–17

Tvergaard, V. (1981): Influence of Voids on Shear Band Instabilities under Plane Strain Conditions. Int. J. Fract. 17, 389–407

Tvergaard, V. (1982): On Localization in Ductile Materials Containing Spherical Voids. Int. J. Fract. 18, 237–252

Needleman, A. (1987): A Numerical Study of Void Nucleation at Carbides. Report of Brown University

Tvergaard, V.; Needleman, A. (1984): Analysis of the Cup-cone Fracture in a Round Tensile Bar. Acta Metall. 32, 157–169

Needleman, A.; Tvergaard, V. (1984): An Analysis of Ductile Rupture in Notched Bars. J. Mech. Phys. Solids 32, 2–15

Chu, C. C.; Needleman, A. (1980): Void Nucleation Effects in Biaxially Stretched Sheets. J. Eng. Mat. Tech. 102, 249–256

Aravas, N. (1987): On the Numerical Integration of a Class of Pressure-Dependent Plasticity Models. Int. J. Num Meth. Eng. 24, 1395–1416

Peirce, D.; Shih, C. F.; Needleman, A. (1984): A Tangent Modulus Method for Rate Dependent solids. Comp. Struct. 18, 875–887

Pan, J.; Saje, M.; Needleman, A. (1983): Localization of Deformation in Rate Sensitive Porous Plastic Solids. Int. J. Fract. 21, 261–278

Needleman, A.; Tvergaard, V. (1991): An analysis of Dynamic Ductile Crack Growth in a Double Edge Cracked Specimen. Int. J. Fract. 49, 41–67

Brocks, W.; Sun, D.-Z.; Honig, A. (1995): Verification of the Transferability of Micromechanical Parameters by Cell-Model Calculations with Visco-Plastic Materials. Int. J. Plast. 11, 971–989

ABAQUS (1994): Version 5.4, Hibbitt, Karlsson and Sorensen Inc.

Perzyna, P. (1966): Fundamental Problems in Viscoplasticity. Adv. Appl. Mech. 9, 243–377

Gilat, A.; Clifton, R. J. (1985): Pressure-Shear Waves in 6061-T6 Aluminum and Alpha-Titanium. J. Mech. Phys. Solids 33, 263–284

Riedel, H. (1986): Fracture at High Temperatures. Pub. Mat. Res. Eng, springer-Verlag

Kachanov, L. M. (1961): Introduction to Continuum Damage Mechanics. Martinus Nijhoff Pub., p. 986

Johnson, J. N. (1981): Dynamic Fracture and Spallation in Ductile Solids. J. Appl. Physics 2812–2825

Freund, L. B. (1992): Dynamic Fracture Mechanics., Cambridge University Press

Hao, S.; Brocks, W. (1996): The Gurson-Tvergaard-Needleman-Model for rate- and Temperature-Dependent Materials with Isotropic and Kinematic Hardenin-Part I: Basic Equations and Results of First Verifications. GKSS, Tech. Note, GKSS/WMG/95/1, GKSS

Aravas, N.; McMeeking, R. M. (1985): Microvoid Growth and Failure in the Ligament between a Hole and a Blunt Crack. Int. J. Fract. 29, 21–38

Bernauer, G. (1995): Bestimmung von Materialparametern des modifizierten Gurson-Modells. TWM-Bericht T 1/95

Brocks, W.; Pusch, G.; Baer, W.; Steglich, D. (1996): Anwendung, mikromechanischer Modelle der Werkstoffschädigung zur gefügeabhangigen Bewertung der Zähigkeit von duktilen Gußeisenwerkstoffen. Final report of DFG Project Pu 104/4 and Br 521/6, Geesthacht and Freiberg

Heerens, J.; Hellmann, D.; Zerbst, U.; Schwalbe, K.-H. (1996): Probendicken- und Ligamenteinschnürung, zwei Größen zur Erfassung der Constraintabhängigkeit von R-Kurve. 28. Tagung, DVM-AKB, Bremen